Research Article Vol. 34, No. 14 / 13 Jul 2026 / *Optics Express* 25578
Optics EXPRESS

Intracavity-SHG telecom modelocked oscillator for compact quantum homodyne detection

CODY W. MART,[1] NICHOLAS V. NARDELLI,[1] MICHAEL B. GRAYSON,[2] LYNDEN K. SHALM,[1,2] AND TARA M. FORTIER[1,*]

[1] *National Institutes of Standards and Technology, 325 Broadway, Boulder, CO 80305, USA*
[2] *University of Colorado, Department of Electrical, Computer, and Energy Engineering, 425 UCB, Boulder, CO 80309, USA*
[*] *tara.fortier@nist.gov*

Abstract: We demonstrate a compact telecom-wavelength modelocked laser source designed for pumping spontaneous parametric downconversion (SPDC), based on an erbium-ytterbium co-doped phosphate glass laser with intracavity second harmonic generation (SHG) to 773.5 nm. Using a 0.4 mm thick β-barium borate crystal, the system produces nearly 35 mW of average power with 191 fs pulses at 773.5 nm. This represents a 1000-fold increase in average power compared to previously reported intracavity SHG modelocked fs-level telecom oscillators (C. Hu, Y. Zhang, Q. Gao, et al., Jap. J. of App. Phys. **59** 080902 (2020)). This architecture provides a path toward homodyne detection of SPDC-generated single photons using a phase-coherent local oscillator derived from the same cavity.

1. Introduction

Accurate measurements of optical quantum states often rely on interference between single photons and a phase-stable local oscillator (LO). The LO is a bright, phase-stable reference laser whose interference with a weak or single-photon-level signal converts quadrature information of the quantum state into measurable intensity differences. Achieving high-fidelity measurements requires the LO to be mode-matched to the single-photon state in its temporal and spectral profiles, spatial mode, and polarization. These requirements place stringent constraints on the spectral purity, timing stability, and coherence of both fields. Such interference-based measurements underpin protocols including balanced homodyne detection for optical quantum tomography [1–3], homodyne detection for Bell inequality violations [4–7], Schrödinger cat state characterization [8,9], and path-entanglement schemes relying on the nonlocality of a single photon [10–12].

A common method of generating either squeezed light or entangled photon pairs is through the second-order nonlinear process of spontaneous parametric downconversion (SPDC). In this process, a single pump photon is converted to a pair of lower frequency signal and idler photons such that energy is conserved. For quantum networking and fiber-based communication protocols it is advantageous for both the SPDC pump and the LO to operate at telecom wavelengths, where fiber loss is minimal [13–17], and to employ pulsed sources to provide timing information, and to support high-visibility interference. For interference between independent sources or mixing with an LO, the SPDC pump should ideally be transform-limited, as chirped, or otherwise non-transform-limited SPDC pump pulses can introduce unwanted temporal and spectral correlations [18]. These correlations reduce the purity of the single-photons and can degrade multiphoton interference by introducing distinguishing information.

Existing methods for generating the required pump and LO fields face significant challenges. A standard method for creating telecom photon pairs is to use a pump laser in the 775 nm range with an SPDC crystal designed for degenerate phase matching, driven by transform-limited modelocked oscillators in the 0.7–1.0 μm range, which provide sufficient peak power to pump SPDC crystals without amplification [19,20]. Performing homodyne measurements on the resulting photons, however, requires a telecom local oscillator at half the pump frequency whose

#587564 https://doi.org/10.1364/OE.587564
Journal © 2026 Received 24 Mar 2026; revised 15 May 2026; accepted 17 May 2026; published 2 Jul 2026

temporal, spectral, spatial, and polarization properties match those of the downconverted photons. Using two independent lasers for the 775 nm pump and the telecom LO therefore requires stabilizing their repetition rates, timing, and pulse shapes, an alignment that is difficult to achieve and maintain. An alternative is to start with a telecom modelocked laser and generate the 775 nm pump via external second-harmonic generation (SHG). Unfortunately, bulk SHG typically requires chirped-pulse amplification and dispersion compensation to obtain transform-limited pulses [21].

An alternative option, explored here, is to exploit the high intracavity powers of free-space oscillators by placing the SHG crystal inside the cavity. The large circulating intracavity pulse energies enable efficient second harmonic generation in comparatively low-$\chi^{(2)}$ materials such as BBO while using short nonlinear crystal lengths, which help mitigate dispersion and nonlinear propagation effects that can lead to pulse distortion. Additionally, the dispersion-managed modelocked cavity supports stable soliton operation without requiring additional external pulse compression or dispersion compensation. While intracavity SHG has been demonstrated for UV [22] and visible [23] pulses, prior implementations in modelocked erbium-doped fiber oscillators have produced only ~10 µW of 775 nm power [24], insufficient for bulk SPDC.

To address this challenge, we present a telecom-wavelength Er/Yb co-doped phosphate-glass modelocked oscillator that can simultaneously produce a time-bandwidth transform-limited pulsed local oscillator at 1547 nm as well as a transform-limited 773.5 nm second harmonic beam that can serve as the pump for SPDC. As both signals are derived in the same cavity, they are inherently matched in repetition rate and remain phase coherent, greatly reducing system complexity for homodyne and related interference-based measurements. Furthermore, the modelocked laser can be locked to other pump/local oscillator systems across a network, supporting future distributed phase-sensitive quantum systems. The oscillator produces up to 34 mW of second-harmonic power with ~191 fs pulses— close to the transform limit—along with a near transform-limited fundamental pulse. This architecture is compatible with the demanding requirements for spectral separability, enhances single-photon generation brightness at 100 MHz repetition rates, and provides a compact, phase-coherent optical source suitable for distributed, phase-sensitive quantum systems.

2. Experimental setup

The oscillator design begins with a 100 MHz telecom-band Er/Yb:P_2O_5 glass free-space linear cavity [25], see Fig. 1. This modelocked laser architecture was selected as the foundation for intracavity SHG because of its high spectral purity [26] and its compatibility with mature, low-cost, commercially available fiber-optic telecom components, enabling a compact and accessible experimental platform. The oscillator is pumped with a fiber Bragg grating locked diode (Gooch and Housego D1611115) that provides stable, sub-1 nm 3 dB bandwidth emission at a center wavelength of 976 nm and a maximum output power of 550 mW. The measured pump polarization extinction ratio is ~17.20 dB. Using ABCD matrix and q-parameter theory, an expected 976 nm beam waist in the gain glass is 24.85 µm in the sagittal plane.

The gain glass is a $4 \times 2 \times 1.9$ mm^3 uncoated rectangular Er/Yb:P_2O_5 glass (TwinStar TSP-21X) oriented at Brewster's angle with propagation along the 2 mm length axis. The doping concentrations are 21 wt% Yb^{3+} and 0.8 wt% Er^{3+}. Measured unabsorbed 976 nm power through the gain glass was 10.3 mW, which is $< 2\%$ of the launched pump and shows adequate absorption of the pump. A half-wave plate centered at 976 nm is used to align the PM-fiber-delivered pump light polarization with the p-polarization orientation on the gain glass to minimize Fresnel reflections.

Robust single-transverse-mode operation is generated by colinearly propagating the telecom signal with a high-brightness 976 nm pump, which is closely matched to and slightly smaller than the signal beam waist within the gain glass. This allows the unpumped region of the gain glass to

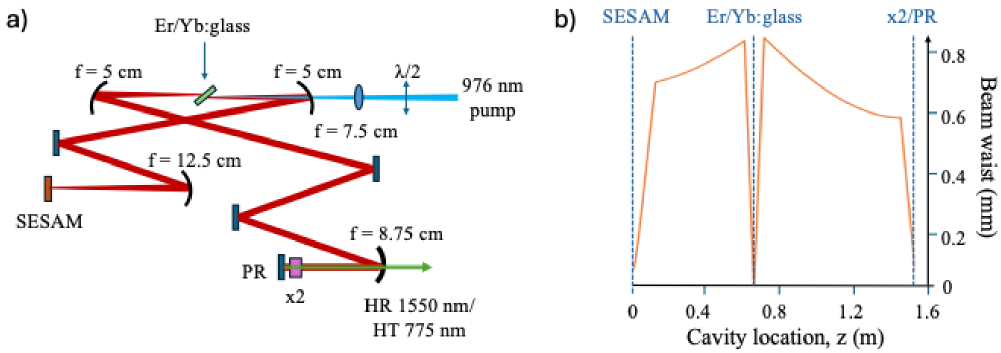

Fig. 1. a) Schematic of the 100 MHz intracavity SHG linear cavity based on an Er/Yb:P_2O_5 glass modelocked laser. The cavity supports three intracavity foci to achieve high fluence at: 1) the SESAM, 2) within the gain glass for self-phase modulation, and at 3) the β-barium borate (BBO) crystal for frequency doubling. The SESAM, gain glass, and BBO (x2) / partial reflector (PR) are located at z = 0m, 0.6415m, and 1.5m, respectively. Three flat turning mirrors provide an estimated −400 fs^2 group-delay dispersion (GDD), while all remaining mirrors exhibit low dispersion (<50 fs^2 absolute GDD). The f = 50 mm dichroic mirrors are highly transmitting at 976 nm and highly reflecting at 1550 nm, while the f = 8.75 cm dichroic mirror is highly transmitting at 775 nm and highly reflecting at 1550 nm. Color code: red = 155X nm, green = 77X nm, blue = 976 nm. b) ABCD matrix simulation of the sagittal beam waist radius as a function of propagation position, showing simulated waist radii of 85.0 μm at the SESAM, 30.5 μm within the gain glass, and 73.1 μm at the BBO crystal.

provide attenuation through ground state Er^{3+} absorption and thus more effectively attenuate higher-order transverse modes.

The oscillator uses a semiconductor saturable absorber mirror (SESAM) to enable modelocking. The SESAM design is based on [27] and features a single Er-doped InGaAs absorbing layer and a lower growth temperature of 475 °C. Both features are included to facilitate shorter pulse generation via ultrafast recombination. The group delay dispersion of the SESAM is -100 fs^2 and the saturation fluence is measured at 180 µJ/cm^2. The SHG crystal is placed directly in front of the partially-reflecting 1550 end mirror to easily match it to the beam waist. The 1550 nm reflectivity is varied by exchanging end mirrors, and ranges from 99.0% to 99.95% reflectivity at 1550 nm.

3. Power scaling

Power scaling in intracavity-frequency-doubled modelocked oscillators requires increasing second-harmonic output while preserving stable mode-locking, pulse duration, spectral purity, and beam quality. In these systems, intracavity nonlinear conversion introduces additional linear and nonlinear losses that can destabilize mode-locking and limit achievable second-harmonic power. Demonstrating stable power scaling while maintaining transform-limited, near-Gaussian spatial modes (see Section 4) therefore establishes the viability of the source and identifies the practical constraints governing intracavity SHG in telecom modelocked oscillators.

Figure 2 depicts the 3 dB bandwidth of the optical spectrum. Also shown is the optical-to-optical efficiency of the modelocked oscillator without the intracavity SHG crystal, as measured through the PR in Fig. 1 a). The data in Fig. 2 represents an oscillator optimized for an output power of 21.4 mW using a 0.1% transmission output coupler. From Fig. 2, we see a modelocking threshold beyond 300 mW pump power as the 3 dB spectral width increases from 0.50 nm to 5.90 nm. In this system, the center wavelength can be tuned from 1559 nm to 1550 nm without the need to swap output couplers (OCs) to higher loss OCs. By adjusting the position of the gain glass relative to the optical resonator beam waist, an imperfect pump/gain glass overlap causes the lasing wavelength to shift to bluer wavelengths at the expense of an approximate 10% reduction in output power. While higher transmission OCs from these oscillators enable higher fundamental output powers nearer to 70 mW [25], the 0.1% transmission OC preserves higher intracavity powers required for intracavity SHG.

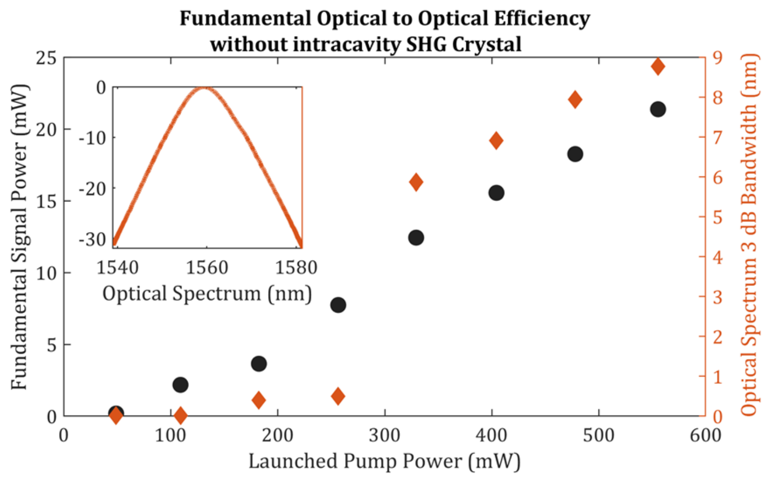

Fig. 2. An optical-to-optical slope efficiency curve showing launched 976 nm pump vs. fundamental modelocked 1559 nm signal output (black circles) along with the 3 dB spectral bandwidth (dark orange diamonds). Inset: log-scale optical spectrum at 550 mW of pump power.

Four type-I phase-matched BBO crystals (0.2, 0.4, 1, and 3 mm nominal thickness) were evaluated for intracavity SHG. The 0.2 mm and 0.4 mm devices consist of optically contacted pairs with orthogonal optic axes [28], resulting in only half the physical thickness contributing to SHG; measured single-pass loss is <0.4% at 1560 nm. Mode-locking was achieved with these low-loss crystals, but not with the monolithic 1 mm and 3 mm crystals (>1.4% loss), indicating that intracavity loss is a limiting parameter for mode-locking in this system.

With the 0.4 mm-thick BBO crystal (NewLight PABBO5040-20.5(I)-AR1550/775) in the cavity, modelocking was achieved with a maximum SHG power of 34 mW. Inclusion of the BBO crystal shifts the modelocked center wavelength from 1559 nm to 1547 nm due to additional linear and nonlinear cavity losses. Operation is highly sensitive to pump power, with variations of tens of mW at 976 nm sufficient to disrupt mode-locking. While this result represents the highest second harmonic powers from an intracavity SHG modelocked telecom oscillator, much higher second harmonic powers can likely be attained by optimizing monolithic SHG crystal lengths while minimizing losses through < 0.1% reflectivity per surface AR coatings, or through Brewster cut crystals with type-0 phase matching to ensure all interacting waves experience zero reflectivity.

To test the SHG saturation effects, the 976 nm pump power was kept constant at the maximum ~550 mW and the OC reflectivity at the fundamental was varied. Figure 3 shows the output power of the fundamental and second harmonic when the OC was varied between 99.0% and 99.95%. The error bars in the plot are associated with uncertainties in the OC reflectivity. The SHG power increased until asymptotically reaching a maximum just above 34 mW, both with the 99.90% and 99.95% reflectivity OC. The measured SHG includes both single- and double-pass contributions due to cavity geometry and high second-harmonic transmission through some optics.

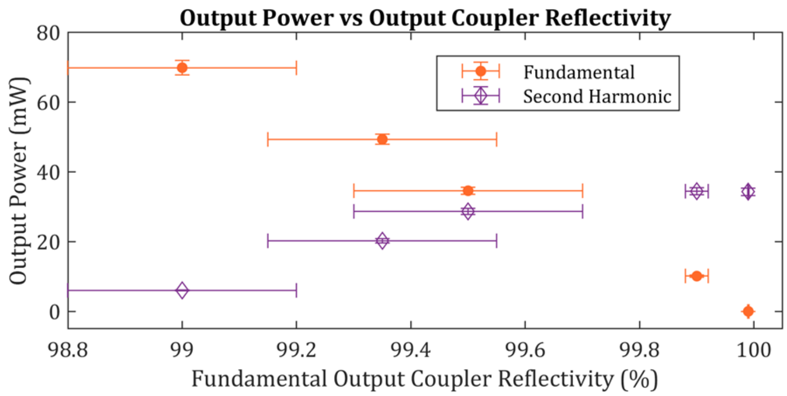

Fig. 3. Output powers of the fundamental (orange circles) and second harmonic (purple diamonds) modelocked laser average power as a function of 1550 nm output coupler reflectivity. Higher output-coupler reflectivity increases the intracavity 1550 nm power, boosting second-harmonic generation and depleting the circulating fundamental field as expected for intracavity SHG.

Finally, power stability measurements were performed by monitoring the output power on 30-minute timescales with ~3 ms optical power sampling intervals. With the SHG crystal inserted, the fundamental output power varied by 0.20% when comparing the measured standard deviation to the mean. This was decreased from the 0.25% fundamental power fluctuations observed without the intracavity crystal. Over the same 30-minute time interval as the fundamental, the second harmonic light varied by 0.32%; which is expected to increase over the fundamental due to its reliance on two fundamental photons for SHG.

4. Beam profile and pulse characterization

Transform-limited operation helps ensures that the LO pulses occupy a well-defined temporal mode with a well-defined spectral phase, a necessary condition for high mode-overlap with the single-photon signal field. Deviations from the transform limit indicate that the pulse exhibits distinguishing temporal information, reducing the LO-signal mode overlap and consequently the fringe visibility and measurement fidelity in interference-based protocols such as balanced homodyne detection. The near-transform-limited pulses depicted in Fig. 4, showing the measured spectrum and intensity autocorrelation traces for the fundamental and SHG signals, indicate that the pulses maintain high temporal coherence and low residual chirp.

Fundamental pulses: To assess pulse fidelity, the measured intensity autocorrelation of the fundamental pulse was directly compared with the transform-limited autocorrelation calculated from the experimentally measured optical spectrum assuming a flat spectral phase. The measured optical spectrum and intensity autocorrelation are shown in Fig. 4 a). The experimentally measured autocorrelation FWHM was (418 ± 9) fs, while the spectrum-derived transform-limited autocorrelation yielded a FWHM of (411 ± 8) fs, indicating that the pulses operate close to the transform limit.

For comparison with standard ultrafast pulse metrics, the fundamental pulse was additionally modeled using a $\mathrm{sech}^2\left(\frac{t}{\tau}\right)$ temporal intensity profile, for which the transform-limited time–bandwidth product is 0.315 and the autocorrelation deconvolution factor is 0.647. Using the measured spectral bandwidth of (1.17 ± 0.01) THz, the inferred pulse duration was

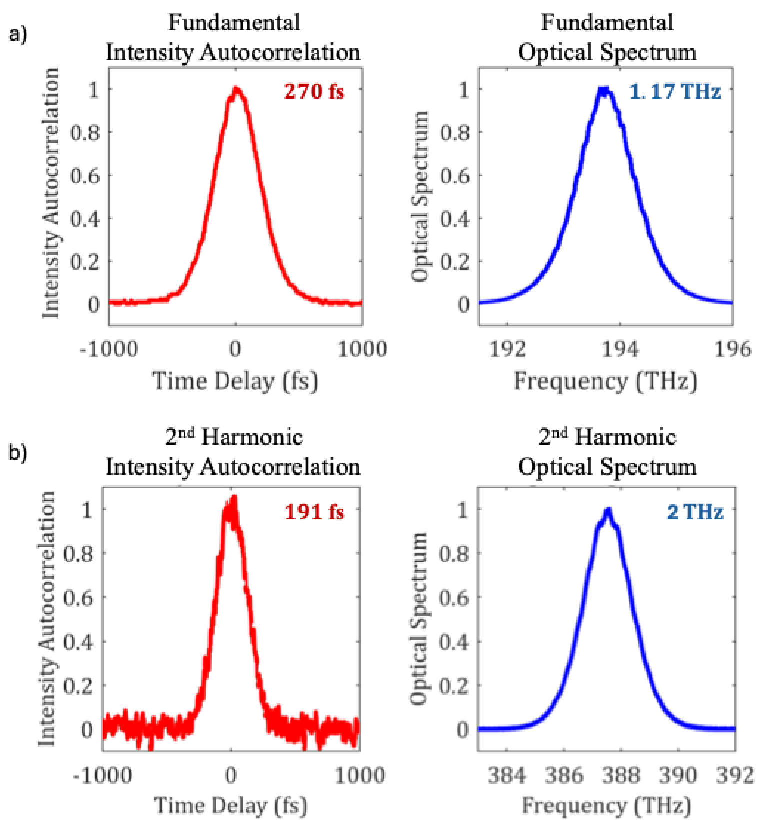

Fig. 4. Intensity autocorrelation (left) and optical spectrum (right) of the a) fundamental pulse and b) second harmonic pulses. Each is plotted on a normalized, linear scale, with the approximate full width half maximum widths indicated.

(270 ± 8) fs, corresponding to a time–bandwidth product of (0.320 ± 0.004), again consistent with near-transform-limited operation.

These results indicate that intracavity dispersion and nonlinear phase accumulation remain well balanced within the oscillator. This pulse quality is important for generating near-transform-limited 773.5 nm second-harmonic pulses for high-purity SPDC and for maintaining strong mode matching between the 1547 nm local oscillator and the generated quantum state.

Second-harmonic pulses: For second-harmonic pulses generated from a sech^2 fundamental pulse, the SHG intensity profile is well approximated by $\text{sech}^4(t/\tau)$, corresponding to a transform-limited time–bandwidth product of 0.366 and an intensity autocorrelation deconvolution factor of 0.675. A full derivation is provided in the Supplement 1.

The second-harmonic optical spectrum and intensity autocorrelation are shown in Fig. 4 b). The measured spectral bandwidth was (2.012 ± 0.007) THz. Applying the sech^4 deconvolution factor yielded an inferred pulse duration of (191 ± 9) fs. This corresponds to a time–bandwidth product of (0.39 ± 0.02), within 6.5% of the transform-limited sech4 value of 0.366, indicating near-transform-limited operation.

To avoid relying solely on an assumed pulse shape, the measured optical spectrum was additionally used to calculate the transform-limited intensity autocorrelation assuming a flat spectral phase. The resulting spectrum-derived autocorrelation FWHM of (236 ± 9) fs exhibits an 18% discrepancy with respect to the measured autocorrelation FWHM of (280 ± 13) fs. This difference likely reflects a combination of factors. The SHG autocorrelation signal is intrinsically weak, and background noise can systematically broaden the measured autocorrelation trace, biasing the inferred pulse duration toward longer values. Additionally, group-velocity mismatch within the BBO crystal introduces dispersion at 773.5 nm that may impart residual chirp on the SHG pulse not captured by the flat-phase assumption used in the spectrum-derived calculation.

Transverse beam profiles of the 1547 nm and 773.5 nm beams are shown in Fig. 5, confirming a near-Gaussian TEM_{00} profile consistent with high spatial mode overlap with the signal field. Together with the pulse characterization above, this verifies that the LO satisfies the mode-matching requirements across temporal, spectral, and spatial degrees of freedom necessary for high-visibility interference-based measurements.

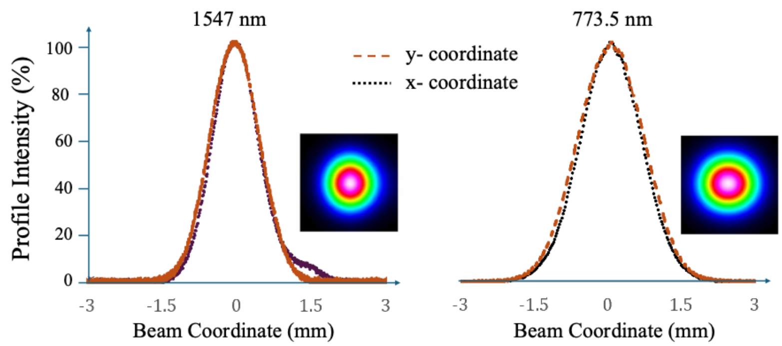

Fig. 5. Transverse beam profiles of the 1547 nm (left) and 773.5 nm (right) beams are shown with 1D lineouts for each orthogonal axis. Inset: 2D beam rendering for each wavelength.

5. SPDC simulations

We next consider the design of the photon-pair generation stage enabled by the intracavity-generated 773.5 nm second-harmonic output. The SHG light pumps a spontaneous parametric down-conversion (SPDC) source producing photon pairs degenerate at 1547 nm, matched to both the local oscillator and the telecom C-band. The crystal geometry, phase-matching configuration, and focusing conditions determine the pair-generation rate, joint spectral correlations, and fiber-coupling efficiency. Engineering the joint spectral correlations is particularly important for generating pure, indistinguishable heralded single photons without spectral filtering. We therefore simulate the SPDC process to identify source parameters that optimize heralded-photon purity and collection efficiency prior to experimental implementation.

Utilizing the SPDC simulations tool available at app.spdcalc.org [29], photon pair generation is estimated along with an ideal nonlinear crystal geometry and poling configuration. A potassium titanyl phosphate crystal with type-II phase matching is used in the simulations. The crystal is 4.0 mm long and is phase-matched using periodic poling using a Gaussian apodization of the poling duty cycle, which suppresses the sinc^2 sidelobes in the joint spectral intensity that arise from uniform poling. The simulated poling period is 46.52 µm with a gaussian apodization of 2100 µm FWHM. This design produces a Schmidt number of 1.002, indicating an almost perfectly separable two-photon state for the 2.012 THz pump bandwidth.

With the above crystal and beam waist radii of 70 µm for the signal and idler and 90 µm for the pump, the estimated photon pair generation is at 321.7 pairs/s/mW. While higher photon pair generation is expected for tighter focusing of the pump, it also broadens the angular spread of the downconverted photons, which reduces fiber-coupling efficiency and can generate heralding events when only one photon of the pair falls within the collection fiber. The chosen beam waists therefore represent a compromise between maximizing the pair rate and ensuring efficient fiber

Optics EXPRESS

collection. The estimated 321.7 pairs/s/mW is on-par with pair generation measurements from thin SPDC crystals and pump beam waist radii nearer to 90 μm [30].

6. Conclusion and outlook

In conclusion, we demonstrated a compact SESAM modelocked Er/Yb:P2O5 oscillator that simultaneously generates both the 1547 nm fundamental and 773.5 nm second-harmonic light that could be applied for SPDC-based photon pair generation and coherent local-oscillator mixing from a common source. This architecture mitigates issues regarding temporal mode overlap while reducing system complexity compared to approaches using independent pump and local-oscillator lasers.

The demonstrated intracavity SHG oscillator produces ~34mW of second-harmonic power, representing an approximately 1000-fold increase over previous femtosecond telecom modelocked oscillators while maintaining near-transform-limited pulse quality.

Intracavity SHG provides advantages over conventional extracavity frequency doubling for ultrashort pulses by leveraging stable soliton dynamics within the mode-locked cavity to balance dispersion and nonlinear phase accumulation. The high intracavity circulating powers additionally enable efficient SHG using short nonlinear crystals, further reducing group-delay and higher-order dispersion. Although intracavity SHG can introduce additional intensity noise through increased cavity loss, this is less critical for SPDC pumping applications, where intensity fluctuations primarily affect source brightness rather than the phase coherence between the LO and generated quantum state.

Further performance scaling is expected through improved nonlinear-crystal engineering, optimized intracavity mode matching, and higher intracavity powers. Stabilization of the repetition rate and carrier-envelope offset would additionally enable ultrahigh phase stability and synchronization between remote oscillators, supporting phase-sensitive quantum measurements and interference experiments involving distributed quantum states.

These results provide a path toward compact, high-brightness telecom quantum light sources and phase-coherent local oscillators for scalable quantum networking and quantum sensing architectures.

Funding. University of Colorado at Boulder's Quantum Engineering Initiative.

Acknowledgements. The authors acknowledge M. Mazurek and M. Stevens for their discussions on phase stable quantum networking architectures. The authors acknowledge R. Mirin and K. Silverman for helpful discussions on SESAM design and characteristics. Certain commercial equipment, instruments, or materials (or suppliers, or software, etc.) are identified in this paper to foster understanding. Such identification does not imply recommendation or endorsement by the National Institute of Standards and Technology, nor does it imply that the materials or equipment identified are necessarily the best available for the purpose.

Disclosures. The authors declare no conflicts of interest.

Data availability. Data underlying the results presented in this paper are not publicly available at this time but may be obtained from the authors upon reasonable request.

Supplemental document. See Supplement 1 for supporting content.

References

1. A. I. Lvovsky, H. Hansen, T. Aichele, *et al.*, "Quantum state reconstruction of the single-photon Fock state," Phys. Rev. Lett. **87**(5), 050402 (2001).
2. H. Hansen, T. Aichele, C. Hettich, *et al.*, "Ultrasensitive pulsed, balanced homodyne detector: application to time-domain quantum measurements," Opt. Lett. **26**(21), 1714–1716 (2001).
3. S. A. Babichev, J. Appel, and A. I. Lvovsky, "Homodyne tomography characterization and nonlocality of a dual-mode optical qubit," Phys. Rev. Lett. **92**(19), 193601 (2004).
4. G. Donati, T. J. Bartley, X.-M. Jin, *et al.*, "Observing optical coherence across Fock layers with weak-field homodyne detectors.," Nat. Commun. **5**(1), 5584 (2014).
5. T. Das, M. Karczewski, A. Mandarino, *et al.*, "Can single photon excitation of two spatially separated modes lead to a violation of Bell inequality via weak-field homodyne measurements?" New J. Phys. **23**(7), 073042 (2021).

Optics EXPRESS

6. T. Das, M. Karczewski, A. Mandarino, *et al.*, "Optimal interferometry for Bell nonclassicality induced by a vacuum-one-photon qubit," Phys. Rev. Appl. **18**(3), 034074 (2022).
7. S.-U. Lee, J. Park, J. Kim, *et al.*, "Single-photon quantum nonlocality: violation of the Clauser-Horne-Shimony-Holt inequality using feasible measurement setups," Phys. Rev. A **95**(1), 012134 (2017).
8. T. Gerrits, S. Glancy, and S. W. Nam, "A balanced homodyne detector and local oscillator shaping for measuring optical Schrödinger cat states," Proc. SPIE **8033**, 80330X (2011).
9. S. U. Shringarpure and J. D. Franson, "Generating entangled Schrödinger cat states using a number state and a beam splitter," Phys. Rev. A **102**(2), 023719 (2020).
10. N. V. Nardelli, D. V. Reddy, M. Grayson, *et al.*, "Phase-stable optical fiber links for quantum network protocols.," Optica Quantum **4**(2), 138–147 (2026).
11. S. M. Tan, D. F. Walls, and M. J. Collett, "Nonlocality of a single photon," Phys. Rev. Lett. **66**(3), 252–255 (1991).
12. O. Morin, J.-D. Bancal, M. Ho, *et al.*, "Witnessing trustworthy single-photon entanglement with local homodyne measurements.," Phys. Rev. Lett. **110**(13), 130401 (2013).
13. P. Caspar, E. Verbanis, E. Oudot, *et al.*, "Heralded distribution of single-photon path entanglement," Phys. Rev. Lett. **125**(11), 110506 (2020).
14. I. Marcikic, H. de Riedmatten, W. Tittel, *et al.*, "Distribution of time-bin entangled qubits over 50 km of optical fiber," Phys. Rev. Lett. **93**(18), 180502 (2004).
15. L. Shen, C. H. Chow, J. Y. X. Peh, *et al.*, "Distributing polarization-entangled photon pairs with high rate over long distances through standard telecommunication fiber," Phys. Rev. Appl. **18**(4), 044075 (2022).
16. N. Gisin and R. Thew, "Quantum communication," Nat. Photonics **1**(3), 165–171 (2007).
17. L. A. Ngah, O. Alibart, L. Labonté, *et al.*, "Ultra-fast heralded single photon source based on telecom technology," Las. & Photonics Rev. **9**(2), L1–L5 (2015).
18. Y. Jeronimo-Moreno and A. B. U'Ren, "Control, measurement, and propagation of entanglement in photon pairs generated through type-II parametric down-conversion," Phys. Rev. A **79**(3), 033839 (2009).
19. D. T. Smithey, M. Beck, M. G. Raymer, *et al.*, "Measurement of the Wigner distribution and density matrix of a light mode using optical homodyne tomography: application to squeezed states and the vacuum," Phys. Rev. Lett. **70**(9), 1244–1247 (1993).
20. Ö. Süzer and T. Goodson III, "Does pump beam intensity affect the efficiency of spontaneous parametric down conversion?" Opt. Express **16**(25), 20166–20175 (2008).
21. M. Grayson, S. Meyer, D. Sorensen, *et al.*, "High-performance source of indistinguishable polarization-entangled photons with a local oscillator reference for quantum networking," arXiv: 2602.10317 (2026).
22. T. V. Andersen, J. Thøgersen, S. R. Keiding, *et al.*, "High-power intracavity frequency doubling of a Ti:sapphire femtosecond oscillator," App. Phys. B **76**(6), 639–644 (2003).
23. T.-M. Liu, S.-P. Tai, and C.-K. Sun, "Intracavity frequency-doubled femtosecond Cr_4+:forsterite laser," App. Opt. **40**(12), 1957–1960 (2001).
24. C. Hu, Y. Zhang, Q. Gao, *et al.*, "Intracavity frequency doubling based on BBO crystals in a mode-locked erbium-doped fiber laser," Jap. J. of App. Phys. **59**(8), 080902 (2020).
25. G. Spühler, L. Krainer, E. Innerhoer, *et al.*, "Soliton mode-locked Er:Yb:glass laser," Opt. Lett. **30**(3), 263–265 (2005).
26. N. V. Nardelli, H. Leopardi, T. R. Schibli, *et al.*, "Optical and microwave metrology at the $10^{(18}$ level with an Er/Yb:glass frequency comb," Las. Phot. Rev. **17**(4), 2200650 (2023).
27. C.-C. Lee, Y. Hayashi, K. L. Silverman, *et al.*, "Monolithic device for modelocking and stabilization of frequency combs," Opt. Express **23**(26), 33038–33043 (2015).
28. P. G. Kwiat, E. Waks, A. G. White, *et al.*, "Ultrabright source of polarization-entangled photons," Phys. Rev. A **60**(2), R773–R776 (1999).
29. L. K. Shalm, "Spdcalc," http://spdcalc.org/ (2022)
30. A. Ling, A. Lamas-Linares, and C. Kurtsiefer, "Absolute emission rates of spontaneous parametric down-conversion into single transverse Gaussian modes," Phys. Rev. A **77**(4), 043834 (2008).